

Supporting Information

From Burst to Controlled Release: Using Hydrogel Crosslinking Chemistry to Tune Release of Micro-Crystalline Active Pharmaceutical Ingredients

Purnima N. Manghnani, Arif Z. Nelson, Kelvin Wong, Yi Wei Lee^c, Saif A. Khan^{*b}, Patrick S. Doyle^{*a}

S1. Nanoemulsion formulation

Preliminary nanoemulsions (NE) were formulated in a continuous phase comprising of 8 wt % PF 127 in water, a dispersed phase of anisole, and a surfactant blend of Tween 80 and Span 80 (HLB = 13.5) at different weight percentages. As seen below, a ternary phase diagram depicts the parameter space explored and the resulting stable emulsion region in gray. The emulsion stability refers to the absence of any phase separation over 24 hours. The points in red depict the parameter space that yields flowable emulsions. These emulsions are obtained at lower

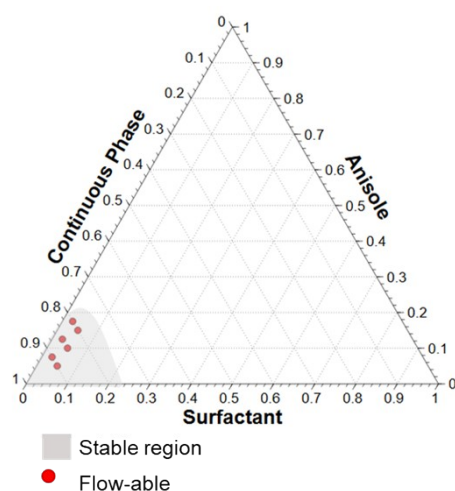


Figure S1. Ternary phase diagram for formation of stable and flowable anisole NE in 8 % PF127 as continuous phase. As the surfactant (HLB = 13.5) concentration increases, the resulting NE becomes increasingly viscous.

surfactant concentrations as a high proportion of surfactant micelles leads to a highly viscous jammed state.

S2. NE micro-droplet stability in fluorinated oil – Role of Pluronic F127

At room temperature, the significant spatial correlation of micelles of 10-12 wt % PF127 solution compared to lower concentrations has been demonstrated by Moretensen et al. through Small-Angle Neutron Scattering¹. Several prior studies have shown that aqueous solutions of PF127 (> 10 wt %) have a microstructure formed through the stacking of micelles^{9,10}. The addition of PF 127 to the continuous phase of the nanoemulsion (NE) enhances its droplet stability at the fluorinated oil-air interface in a concentration-dependent manner. Here, the concentration-dependent interaction of PF127 micelles was investigated using Nile Red as a micropolarity indicator^{2,3}. Nile Red (NR) has been shown to interact with polyethylene oxide (PEO) segments of surfactant micelles and not reside within the hydrophobic micelle core. Therefore, as micelle interaction increases, the NR molecules would experience different micropolarity and exhibit a change in fluorescence. NR was dispersed in varying concentrations of PF127 solutions (0.1 mg/mL of NR). As shown in Figure S2a and b, the fluorescence of NR increased as the concentration of PF127 increased. The increase in emission intensity was notable at 8-10 wt % PF127. As the concentration of the PF127 increases, the PEO segments of the neighboring micelles begin interacting and ordering on a crystalline lattice. The Nile Red aggregates adhered to the PEO chains experience a change in polarity as a result of this ordering causing

them to fluoresce. More specifically, at low concentrations (< 8 wt %), the PEO chains are fully hydrated and the Nile Red experiences higher polarity leading to low fluorescence. As the number of micelles increases, the PEO chains begin overlapping, reducing their degree of hydration and reducing the microenvironment's polarity around the NR aggregates.

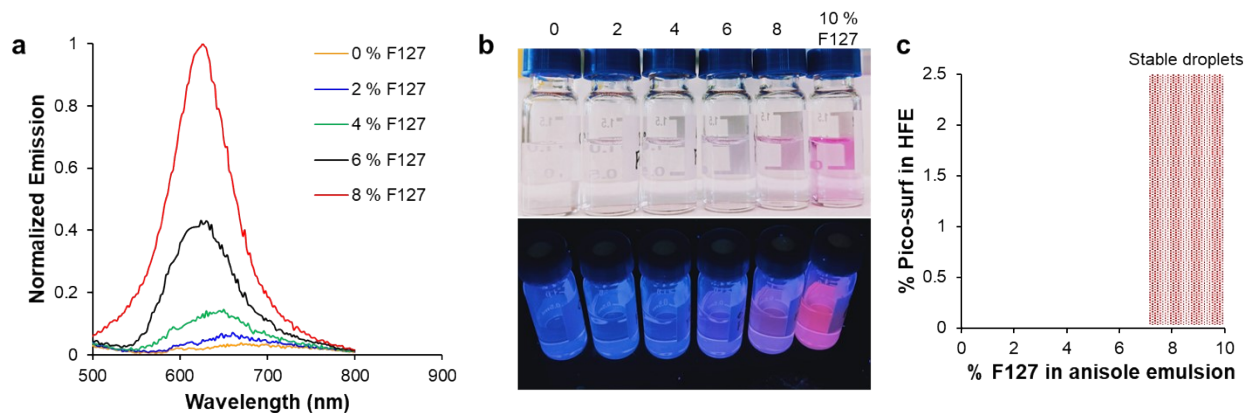


Figure S2. a. Fluorescence spectra of micropolarity indicator Nile Red in varying concentration of Pluronic F127, b. Images of vials containing Nile Red in varying concentration of Pluronic F127, c. Nanoemulsion micro-droplet stability as a function of oil phase surfactant, Pico-surf in HFE-7500 and percentage of F127 in the aqueous phase of NE at 15 % anisole.

For the high-throughput formulation of the NE into microparticles, the NE was step-emulsified in micro-droplets in a fluorinated oil (HFE7500) bath containing 0.03 % v/v Pico-surf. Due to the density difference between the fluorinated oil and the NE, the micro-droplets rose to the surface of the oil bath. It was found that if the NE continuous phase had low concentration of Pluronic F127, the droplets coalesced at the air-oil interface (Video S1). However, at higher concentrations of Pluronic F127 (8-10 wt %), the micro-droplets were stable on the air-oil interface (Video S2) for up to 2 minutes (Figure S2c). This granted time for cross-linking and micro-hydrogel formation to occur.

S3. Anisole extraction from micro-hydrogels

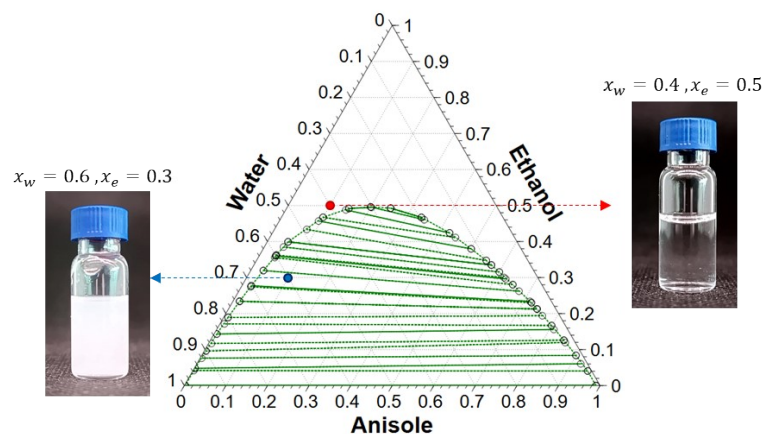


Figure S3. Ternary phase diagram dictating the amount of water-ethanol system for anisole extraction from micro-hydrogels. Vial images depict typical single-phase and two-phase regions of the phase diagram.

The extraction of anisole from the micro-hydrogels was performed in an anti-solvent sink composed of varying concentrations of ethanol in water. The extraction of anisole was governed by the ternary phase diagram of anisole, water, and ethanol. It was imperative to have the composition of the three phases such that it existed above the binodal line, therefore, forming a single phase.

$$\text{Volume of each microparticle} = \frac{4}{3}\pi r^3 = 2.4 \times 10^{-9} \text{ m}^3$$

$$\text{Volume of anisole in each microparticle} = 0.36 \times 10^{-9} \text{ m}^3 = 0.36 \mu\text{L}$$

$$\text{Volume of anti - solvent sink} = 10 \text{ mL}$$

Minimum mole fraction of components for single phase formation from ternary phase diagram, obtained through COSMO-RS-

$$X_{\text{water}} = 0.98, X_{\text{ethanol}} = 0.01, X_{\text{anisole}} = 0.01 \quad (G^{\text{mix}} < 0)$$

For an anti-solvent sink containing 5 % v/v ethanol, 9.5 mL water was mixed with 0.5 mL of ethanol. A total of 200 micro-hydrogels were placed in the sink and placed on an orbital shaker at 100 rpm. The mole fraction of the bath post-extraction was calculated as follows-

$$X_{\text{water}} = 0.982, X_{\text{ethanol}} = 0.016, X_{\text{anisole}} = 0.001$$

which possessed much lower anisole than the theoretical miscibility molar fraction.

S4. Swelling ratio of bulk hydrogels

PEGVs-DT and PEGAc-DT bulk gels were synthesized with three formulation combinations – 1) Control PEG gels comprising of PEGVs-DT or PEGAc-DT, 2) the PEGVs-DT or PEGAc-DT gel with PF 127 in the aqueous phase and 3) the nanoemulsion of anisole in the continuous phase of PEG pre-polymers, PF 127 and surfactants (See experimental section). The polymerization was carried out in microwells holding HFE7500 with 0.25 % v/v trimethylamine. 50 μL of pre-polymer was carefully dripped into the microwell. The resulting gels were washed in ethanol and water. The hydrogel discs were dried under vacuum overnight and were weighed immediately (m_{dry}). The swelling ratio of the bulk gels was obtained by soaking the dry gels in water for 2 days. The wetted hydrogels were retrieved, the excess water was wicked from the surface using kimwipes, and were weighed (m_{wet}). The swelling ratio was calculated according to the formula-

$$\text{Swelling ratio} = \frac{m_{\text{wet}} - m_{\text{dry}}}{m_{\text{dry}}}$$

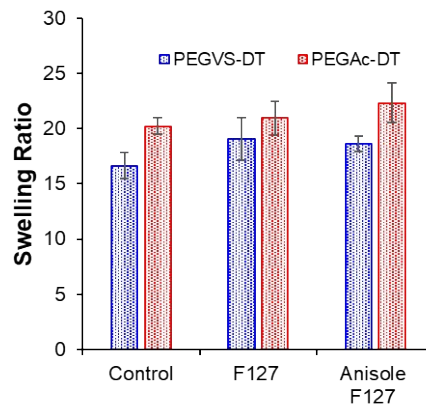


Figure S4. Swelling ratios of bulk PEGVs-DT and PEGAc-DT gels fabricated with PEGVs-DT or PEGAc-DT (control), PEGVs-DT or PEGAc-DT with F127 and gelled nanoemulsion. }

S5. Fabrication of blank micro-hydrogels

Blank micro-hydrogels were fabricated by cross-linking the NE solution with the PEGVs-DT backbone containing the anisole dispersed phase without any fenofibrate (Fen) in it. The micro-hydrogels were fabricated following the same procedure as that for the Fen-loaded ones. They were then equilibrated in 5 % ethanol anti-solvent. The resulting micro-hydrogels were characterized using optical microscopy in wet condition and FESEM in dry condition.

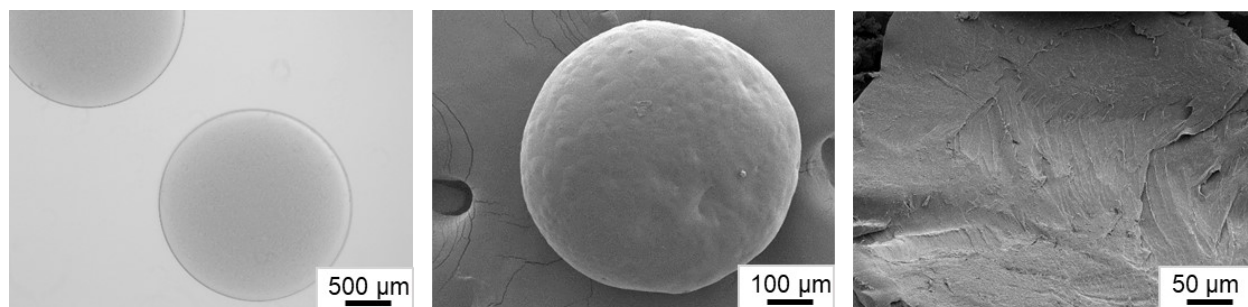


Figure S5. Optical micrograph of blank PEGVs-DT micro-hydrogels formulated without Fen in anisole in wet condition and FESEM images of the blank PEGVs-DT micro-hydrogel surface and cross-section.

S6 and S7. Morphology of Fen-loaded micro-hydrogels

Fen-loaded micro-hydrogels (PEGVs-DT and PEGAc-DT) prepared through cross-linking of NE micro-droplets were subjected to solvent extraction in anti-solvent of varying ethanol concentration. The concentration of ethanol was varied from 5 % v/v to 80 % v/v. As the anisole got extracted out of the micro-hydrogel in the anti-solvent, the Fen precipitated in the micro-hydrogel environment. The micro-hydrogels were filtered 30 minutes post-solvent-extraction and placed in DI water for another 30 minutes. A distinct variation in Fen crystal morphology within the micro-hydrogels was observed as the ethanol concentration in the sink varied (Figure S6 and S7). This can be appreciated by comparing the Fen-loaded micro-hydrogels with blank micro-hydrogels formulated without Fen in anisole (Figure S5). In Figures S6a and S7a, optical microscopy images of the micro-hydrogels in the anti-solvent and FESEM characterization of the dried micro-hydrogels are presented. At 5-40 % v/v ethanol concentration of the anti-solvent sink, Fen precipitated throughout the particle cross-section. A closer look at the FESEM characterization, however, showed larger Fen crystals on the surface of micro-hydrogels obtained at the 40 % ethanol anti-solvent condition compared to the 5 % ethanol anti-solvent. In distinct contrast to the lower ethanol anti-solvent conditions, the Fen crystals within the micro-hydrogel cross-section at higher ethanol conditions (60-80%) presented higher

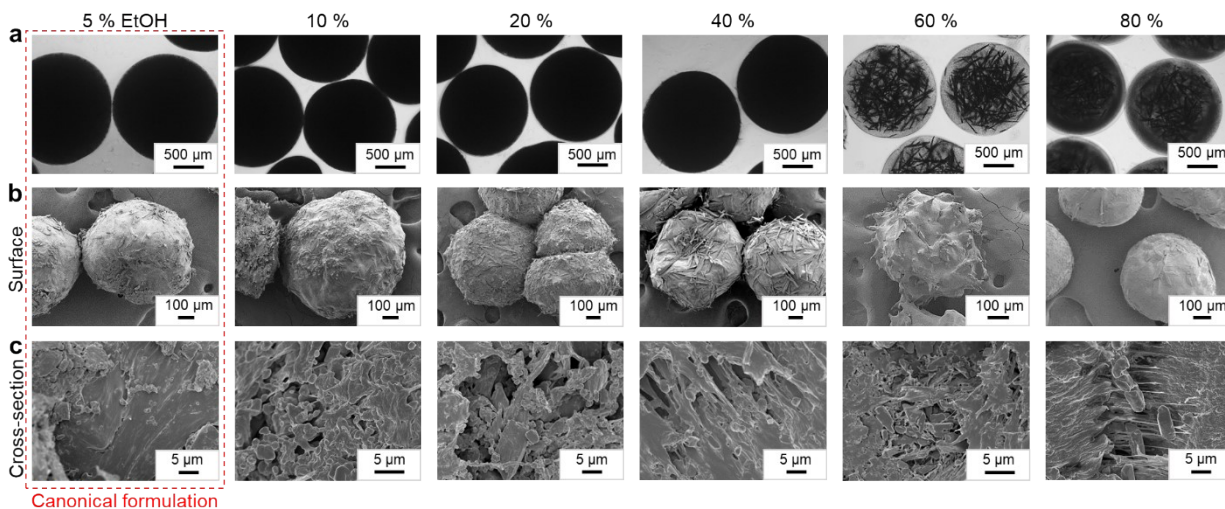


Figure S6. Optical micrographs and FESEM characterization of Fen loaded PEGVs-DT micro-hydrogels after solvent exchange. **a.** Optical micrographs of Fen PEGVs-DT micro-hydrogels after solvent exchange in anti-solvent sinks with varying ethanol (EtOH) concentrations, **b.** FESEM images of Fen PEGVs-DT micro-hydrogels after drying, **c.** FESEM images of PEGVs-DT micro-hydrogel cross-sections showing Fen crystals embedded in the polymer matrix.

aspect ratios, and almost no Fen crystals were found on the micro-hydrogel surface. Variation of the anti-solvent sink composition affected the degree of supersaturation experienced by the Fen molecules in two possible ways – change in anisole extraction rate and change in amount of Fen solvated in ethanol. These directly impacted the crystal nucleation and growth dynamics. While a high degree of supersaturation at lower ethanol concentration led to high nucleation rate and smaller Fen crystals in the micro-hydrogels, a lower degree of supersaturation at high

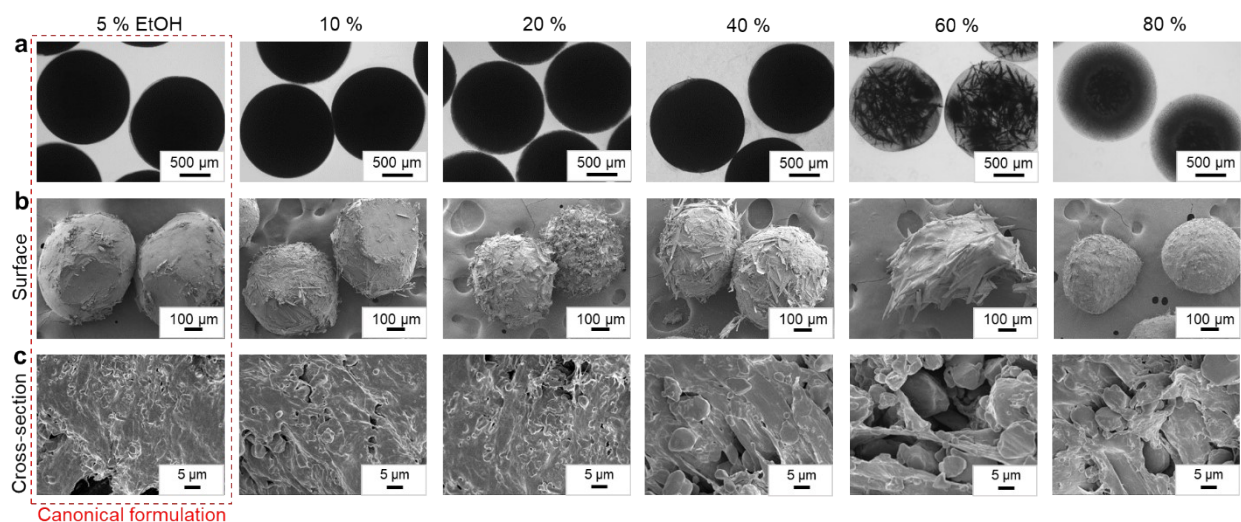


Figure S7. Optical micrographs and FESEM characterization of Fen loaded PEGAc-DT micro-hydrogels after solvent exchange. a. Optical micrographs of Fen PEGAc-DT micro-hydrogels after solvent exchange in anti-solvent sinks with varying ethanol (EtOH) concentrations, b. FESEM images of Fen PEGAc-DT micro-hydrogels after drying, c. FESEM images of Fen PEGAc-DT micro-hydrogel cross-sections showing Fen crystals embedded in the polymer matrix.

ethanol concentration led to larger Fen crystals indicating a crystal growth dominance.

S8 and S9. Solid-state outcome of Fen and PEG in the composite micro-hydrogels

The crystallinity of the Fen loaded PEGVs-DT micro-hydrogels (Fen PEGVs-DT) extracted with ethanol anti-solvent (5-80 %) was compared with neat PEGVs-DT micro-hydrogels and raw Fen powder in Figure S8. The powder X-ray diffraction (PXRD) profile of Fen PEGVs-DT showed characteristic peaks of both PEG and Fen form I indicating presence of crystalline drug and polymer. Furthermore, the Fen PEGVs-DT micro-hydrogels extracted at different anti-solvent conditions were compared using differential scanning calorimetry (DSC). The DSC curves for all extraction conditions of the micro-hydrogels showed two endotherms at ~ 48 °C and ~ 74 - 76 °C distinct from the melting points of the individual Fen and PEG components. A right-shift of about 2 °C was observed in the second endotherm between the 5 % and 60 % ethanol formulations, a possible outcome of the varying Fen morphology. Additionally, an overlap of individual PXRD peaks of both PEGVs-DT and Raw Fen were observed for all the formulations.

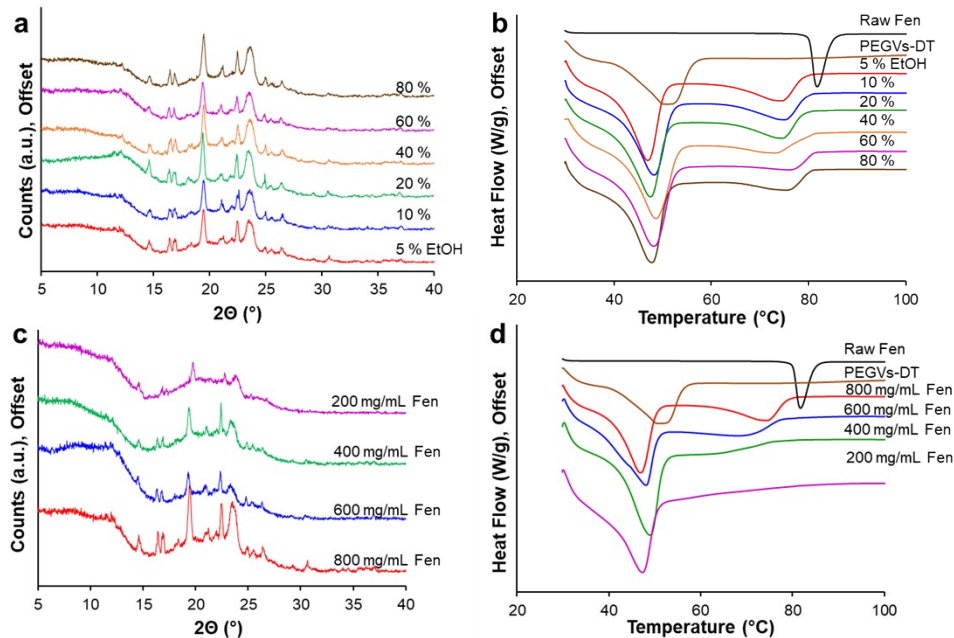


Figure S8. Characterization of Fen crystals in PEGVs-DT hydrogel matrix. a. PXR curves of Fen PEGVs-DT micro-hydrogels subjected to different anti-solvent sink conditions , b. DSC thermograms of the Fen PEGVs-DT micro-hydrogels subjected to different ethanol (EtOH) anti-solvent sink conditions in comparison to raw Fen and PEGVs-DT, c. PXR curves of Fen PEGVs-DT micro-hydrogels prepared with varying Fen concentration in the anisole phase (800-200 mg/mL), d. DSC thermograms of Fen PEGVs-DT micro-hydrogels prepared with varying Fen concentration in the anisole phase (800-200 mg/mL) with 5 % EtOH anti-solvent.

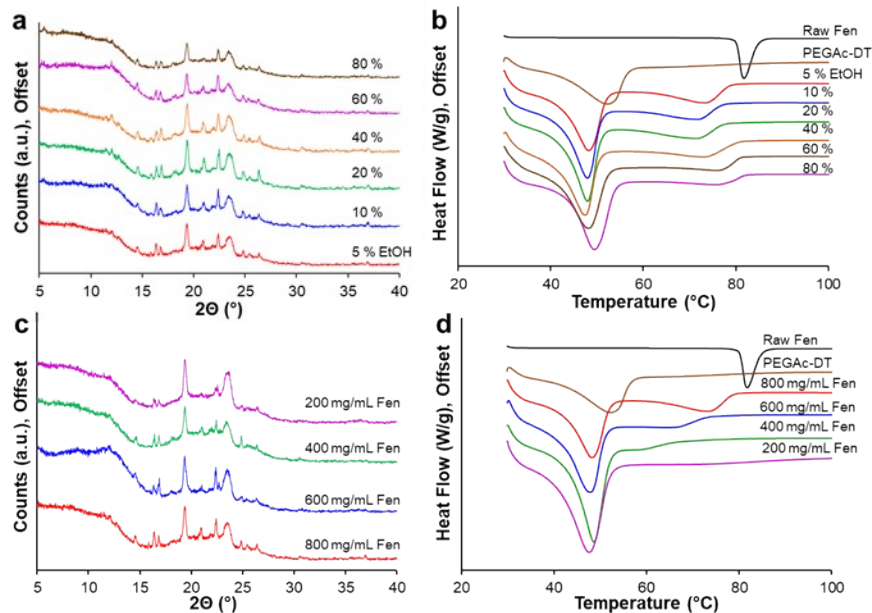


Figure S9. Characterization of Fen crystals in PEGAc-DT hydrogel matrix. a. PXR curves of Fen PEGAc-DT micro-hydrogels subjected to different anti-solvent sink conditions , b. DSC thermograms of the Fen PEGAc-DT micro-hydrogels subjected to different ethanol (EtOH) anti-solvent sink conditions in comparison to raw Fen and PEGAc-DT, c. PXR curves of Fen PEGAc-DT micro-hydrogels prepared with varying Fen concentration in the anisole phase (800-200 mg/mL), d. DSC thermograms of Fen PEGAc-DT micro-hydrogels prepared with varying Fen concentration in the anisole phase (800-200 mg/mL) with 5 % EtOH anti-solvent.

S10. Eutectic formation

An important feature of PEG is that its repeating unit contains a hydrophobic region of ($-CH_2-CH_2-$) and one hydrogen bonding site ($-O-$). The Raman spectrum of a dilute PEG (M_w 6000 Da) solution has shown that PEG molecules retain their helical crystalline structure when dissolved, albeit less ordered⁴. This indicates that the high-molecular-weight PEGs used in our study possess crystalline domains even in the hydrated micro-hydrogel⁵. We hypothesize that these crystalline domains can interact with the lipophilic nucleating Fen in the micro-hydrogel environment leading to a combined crystalline microstructure.

From another perspective, for a solid system comprising a crystalline drug with a higher melting point than the crystalline polymeric carrier, the drug must be soluble in the molten polymer for it to be eutectic⁶. The eutectic formation between a drug and a polymer can therefore be evaluated by quantifying the solubility of the drug in the molten state of the polymer. Theoretically, drugs with low melting temperatures, low heat of fusion, high cLog P, and strong interactions with the polymer will have high solubility in the molten polymer. Properties of Fen and PEG (M_w 10000 Da) from the literature are stated in the table below^{6,7}. Despite the lack of specific interactions between Fen and PEG, Fen possesses a low melting point and low heat of fusion which can result in the reduced crystallizing propensity for Fen molecules. Furthermore, Fen has a high cLog P value and a melting temperature that is fairly close to that of PEG. The Flory-Huggins interaction parameter between PEG (M_w 6000 Da) and Fen has been estimated to be 0.27, which indicates that adhesive forces of interaction between PEG and Fen are stronger than the cohesive forces⁸. This was experimentally corroborated for solid dispersions of Fen in PEG 6000⁹.

Compound	Molecular weight	T_m (°C)	ΔH_f (kJ/mole)	cLogP
Fenofibrate	361	80.2	34	4.43
PEG	10000	57.5	1828.6	

Table S1. Properties of Fenofibrate and PEG

We further probed the solubility of Fen in PEG using COSMO-RS. The monomeric analogs of PEG, ethylene glycol, diethylene glycol, and triethylene glycol from the COSMO-RS database were used to estimate their Gibbs free energy of mixing with Fen. As the chain length increased, the system exhibited negative free energy of mixing for all proportions of Fen and the monomers (Figure S10).

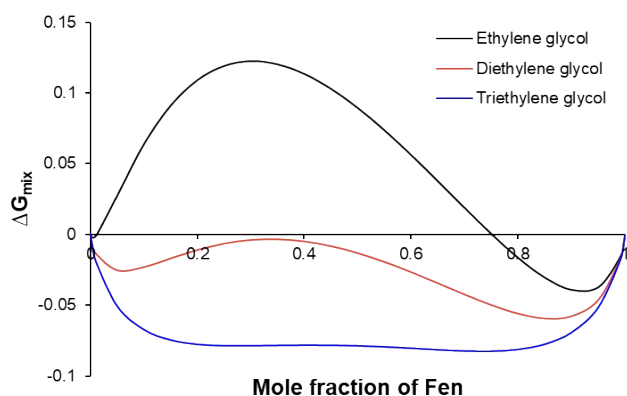


Figure S10. Gibbs free energy of mixing obtained from COSMO-RS for Fen and Ethylene glycol, diethylene glycol and triethylene glycol as proxies for PEG.

S11. Drug load in micro-hydrogels

The Fen mass loading (w/w) in the micro-hydrogels was determined using Cary 60 UV-Visible spectrophotometer. Approximately 4 mg of the composite microhydrogels were placed in ethanol and allowed to dissolve for 2 hours. The loading was determined by comparing the measured UV-visible spectrum maxima at 290 nm to a calibration curve obtained in the concentration range of 1 to 25 $\mu\text{g mL}^{-1}$ Fen dissolved in ethanol (Figure S11). The calibration

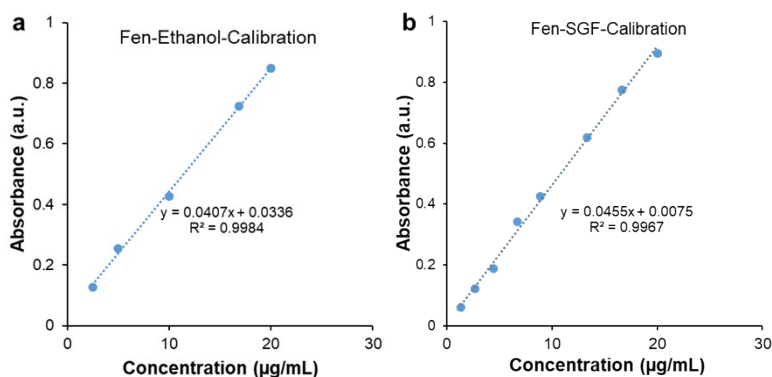


Figure S11. Calibration curves of Fen concentration measured in a. ethanol and b. SGF obtained using UV-Visible absorbance measurement.

% of ethanol in anti-solvent	Fen in PEGVs-DT (% w/w)	Fen in PEGAc-DT (% w/w)
5 %	55.05 ± 3.50	51.17 ± 5.32
10 %	49.19 ± 5.40	45.25 ± 4.70
Concentration of Fen in anisole (mg/mL)	Fen in PEGVs-DT (% w/w)	Fen in PEGAc-DT (% w/w)
200	46.29 ± 5.59	40.01 ± 5.84
400	36.11 ± 4.32	32.98 ± 8.51
600	47.13 ± 5.27	43.26 ± 5.44
800	55.05 ± 3.50	51.17 ± 5.32

Table S3. Fen load in PEG micro-hydrogels as a function of Fen concentration in anisole (DP of NE). The % of ethanol in anti-solvent sink was maintained at 5 % for all the formulations.

curve for Fen in SGF was established by dissolving excess Fen in SGF and filtering the solution prior to UV-visible spectrophotometry.

Polymer composition	Fen in micro-hydrogel (% w/w)
PEGVs-DT	55.05 ± 3.50
75 % PEGVs – 25 % PEGAc- DT	51.23 ± 2.15
50 % PEGVs – 50 % PEGAc -DT	53.17 ± 4.42
PEGAc-DT	51.17 ± 5.32

Table S4. Fen load in PEG micro-hydrogels as a function of the polymer composition. The total polymer concentration in the continuous phase was maintained at 10 % w/v. The % of ethanol in anti-solvent sink was maintained at 5 % for all the formulations.

S12 and S13. Drug dissolution

The Korsmeyer-Peppas model was used to analyze the diffusional release from the PEGVs-DT micro-hydrogels. The model evaluates the release of the initial release ($C/C_0 < 0.6$) according to the equation:

$$\frac{C}{C_0} = Kt^n$$

where C/C_0 is the fraction of the release drug at time t , K is the rate constant and n is the release exponent. The value of n characterizes the release mechanism from the polymeric composite. For the PEGVs-DT micro-hydrogels formulated with 200 mg/mL of Fen in anisole showed $n < 0.45$, which indicated a Fickian diffusion regime. This indicates that the drug diffusion may proceed faster than the polymer relaxation. For the higher concentration formulations, $n > 0.45$ indicated non-Fickian drug release. Here, the drug diffusion and polymer relaxation occurs at competing time scales.

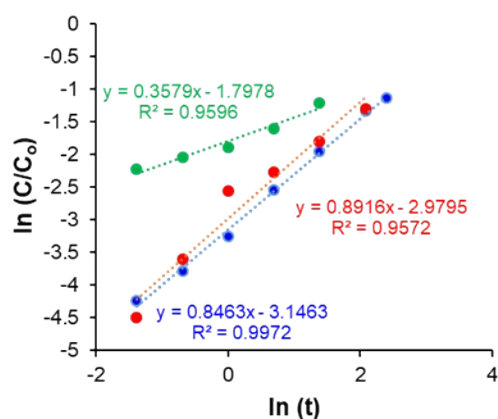


Figure S12. Korsmeyer-Peppas model fit ($C/C_0 < 0.6$) for the dissolution profiles of Fen embedded in PEGVs-DT micro-hydrogels prepared with varying Fen concentration in the anisole phase – 800 (red), 400 (blue) and 200 mg/mL (green); n is the slope of the linear fit and K is the intercept.

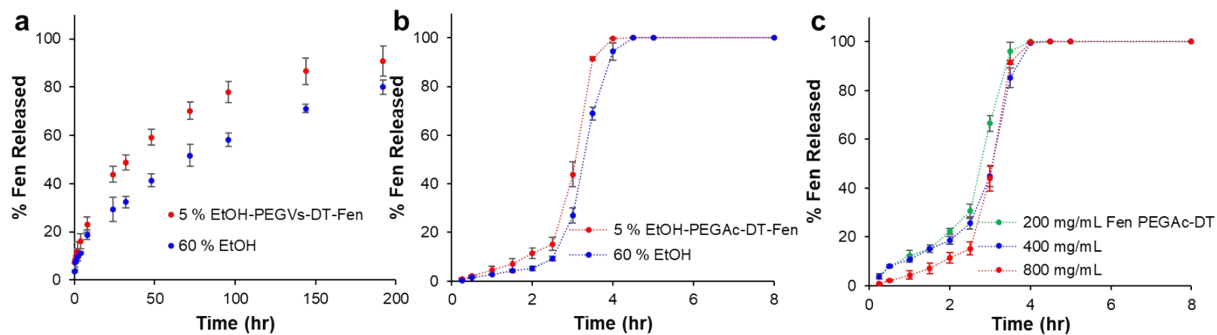


Figure S13. Dissolution in SGF of Fen embedded in a. PEGVs-DT micro-hydrogels subjected to different ethanol (EtOH) anti-solvent sink conditions of 5 % EtOH and 60 % EtOH, b. PEGAc-DT micro-hydrogels subjected to different ethanol (EtOH) anti-solvent sink conditions of 5 % EtOH and 60 % EtOH c. PEGAc-DT micro-hydrogels prepared with varying Fen concentration in the anisole phase (800-200 mg/mL).

S14. Stability of the micro-hydrogels

We have evaluated the stability of the Fen loaded PEGVs-DT and PEGAc-DT micro-hydrogels (800-400 mg/mL Fen in anisole) stored in dry conditions at 20 °C and 43 % relative humidity through differential scanning calorimetry (DSC). The DSC curves shown in the figure below indicate that the solid-state outcome does not change significantly at the 180-day time point.

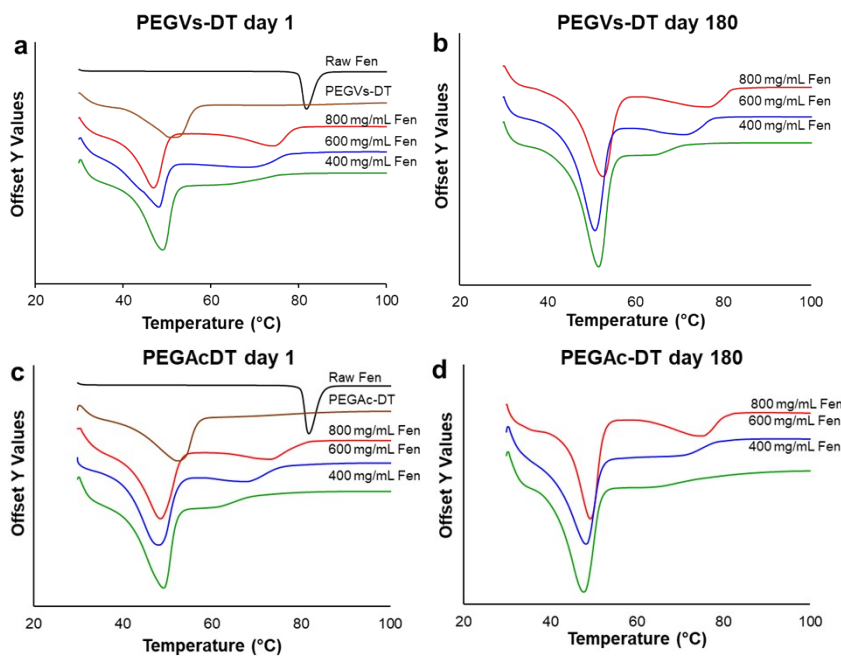


Figure S14. DSC thermograms of the Fen PEGVs-DT micro-hydrogels at a. day 1, b. day 180 and Fen PEGAc-DT microhydrogels at c. day 1 and d. day 180.

References

1. Mortensen K, Talmon Y. Cryo-TEM and SANS Microstructural Study of Pluronic Polymer Solutions. *Macromolecules*. 1995 Dec 1;28(26):8829–34.
2. Swain J, Mishra AK. Nile red fluorescence for quantitative monitoring of micropolarity and microviscosity of pluronic F127 in aqueous media. *Photochem Photobiol Sci*. 2016;15(11):1400–7.
3. Kurniasih IN, Liang H, Mohr PC, Khot G, Rabe JP, Mohr A. Nile Red Dye in Aqueous Surfactant and Micellar Solution. *Langmuir*. 2015 Mar 10;31(9):2639–48.
4. Kuzmin V V, Novikov VS, Ustynyuk LY, Prokhorov KA, Sagitova EA, Nikolaeva GY. Raman spectra of polyethylene glycols: Comparative experimental and DFT study. *J Mol Struct*. 2020;1217:128331.
5. Eagland D, Crowther NJ, Butler CJ. Interaction of poly(oxyethylene) with water as a function of molar mass. *Polymer (Guildf)*. 1993;34(13):2804–8.
6. Vipagunta SR, Wang Z, Hornung S, Krill SL. Factors Affecting the Formation of Eutectic Solid Dispersions and Their Dissolution Behavior. *J Pharm Sci*. 2007 Feb 1;96(2):294–304.
7. Kou Y, Wang S, Luo J, Sun K, Zhang J, Tan Z, et al. Thermal analysis and heat capacity study of polyethylene glycol (PEG) phase change materials for thermal energy storage applications. *J Chem Thermodyn*. 2019;128:259–74.
8. Thakral S, Thakral NK. Prediction of Drug–Polymer Miscibility through the use of Solubility Parameter based Flory–Huggins Interaction Parameter and the Experimental Validation: PEG as Model Polymer. *J Pharm Sci*. 2013;102(7):2254–63.
9. Ming-Thau S, Ching-Min Y, Sokoloski TD. Characterization and dissolution of fenofibrate solid dispersion systems. *Int J Pharm*. 1994;103(2):137–46.